PHYSICAL REVIEW B **73**, 155330 (2006)

# Terahertz radiation from InAs induced by carrier diffusion and drift

Kai Liu, Jingzhou Xu, Tao Yuan, and X.-C. Zhang*
*Center for THz Research, Rensselaer Polytechnic Institute, Troy, New York 12180, USA*
(Received 22 August 2005; revised manuscript received 13 December 2005; published 26 April 2006)

Terahertz (THz) radiation from a (100) oriented InAs surfaces is dominated by the photo-Dember effect. The strength of the radiation is influenced by screening the radiation with doped carriers. When irradiated by femtosecond pulses, the wafer with the lowest doping concentration radiates THz power nearly two orders higher than the wafer with highest doping concentration. With identical optical excitation and same doping concentration, a *p*-type InAs generates stronger THz waves than an *n*-type InAs due to the weaker screening effect. The low doping *p*-type InAs ($1\times10^{16}$ cm$^{-3}$) sample is the strongest THz wave emitter among all the unbiased semiconductors we have ever tested with a Ti:sapphire laser oscillator. The drift-diffusion equation (DDE) is used in the study of carrier drift and diffusion as well as subsequent THz radiation from InAs wafers. The calculation explains well the experimental observation of the relationship between a THz electric field and the doping properties of InAs. The physical pictures of the carrier drift and diffusion characteristics in InAs surfaces are also clearly provided in this report.

DOI: 10.1103/PhysRevB.73.155330 PACS number(s): 72.20.Jv, 41.60.−m, 42.65.Re, 42.72.Ai

## I. INTRODUCTION

Pulsed terahertz (THz) radiation from semiconductor surfaces using femtosecond lasers has been studied extensively in recent years. Herein, the mechanisms of THz radiation from these semiconductor surfaces are investigated. With ultrafast laser pulses incident on the semiconductor surface, ultrafast charge transport is driven either by the intrinsic surface electric field of the semiconductor[1] or by an induced concentration gradient of the surface charges due to photoexcitation.[2] The electron transport subsequently leads to the emission of a THz transient.

It has been reported that some III-V semiconductors, such as GaAs, emit THz waves from accelerated carriers driven by the conduction band bending at the semiconductor surface.[1] Kersting *et al.*[3,4] further reported the contribution of cold plasmon oscillation in *n*-type GaAs for THz radiation. InP generates THz waves at a low excitation density when driven by the built-in surface field and conversely generates waves at a high excitation density with the photo-Dember effect.[5] Some narrow band-gap III-V semiconductors, such as InAs and InSb with the band gaps only 0.35 and 0.17 eV, emit THz waves differently. An (100) oriented InAs radiates THz waves mainly by carrier transport driven by the photo-Dember field.[6,7]

InAs has been reported to generate THz waves with the intensity an order of magnitude higher than those of wide band-gap semiconductors such as InP and GaAs (Ref. 8) under similar experimental conditions. This is due to the following reasons: the electron mobility of InAs is much larger than that of GaAs; the effective electron mass of InAs is much smaller compared to that of GaAs, as shown in Table I; the rest energy of photoexcited electron in InAs is relatively large since the bandgap of InAs is small; the penetration depth for an 800 nm laser pulse in InAs is only about 150 nm, which is much smaller than 1 $\mu$m in GaAs. The concentration gradient for the photoexcited carriers on the InAs surface should therefore be much larger than in the GaAs surface under the same incident laser power. It is reasonable to conclude that InAs wafer radiates more THz power in comparison to GaAs driven by the carrier concentration gradient. The higher order THz wave enhancement of InAs in the presence of a magnetic field determines its importance as a powerful THz wave emitter.[9,10]

In a recent paper, Adomavicius *et al.*[11] report THz wave radiation by optical rectification[12] that the (111) oriented *p*-type InAs with a low carrier concentration of $10^{16}$ to $10^{17}$ cm$^{-3}$ shows larger THz power compared with *n*-type InAs due to an electric-field-induced optical rectification effect in the surface depletion layer. For (100) oriented InAs with laser pulses incident at about 45° to surface normal, THz wave radiations occur mainly from the arising carrier transport which is driven by the photo-Dember field. Little is contributed by optical rectification in this case.

In this paper, we report the observations of THz radiation from a series of *n*-type and *p*-type InAs wafers with different doping concentrations. THz radiations from different types of InAs are simulated with the drift diffusion equation based on a photo-Dember mechanism.

TABLE I. Parameters for DDE calculation, those with asterisks are cited from *Handbook Series on Semiconductor Parameters*, Vols. 1 and 2 edited by M. Levinstein, S. Rumyantsev, and M. Shur (World Scientific, London, 1999).

| | |
|---|---|
| Time evolution for the calculation | 1 ps |
| Calculated sample thickness | 1 $\mu$m |
| Excess energy of electron | 0.5 eV |
| Lattice temperature | 300 K |
| Electron mobility* | 33 000 cm$^2$ V$^{-1}$ s$^{-1}$ |
| Hole mobility* | 460 cm$^2$ V$^{-1}$ s$^{-1}$ |
| Intrinsic carrier concentration* | $10^{15}$ cm$^{-3}$ |
| Dielectric constant* | 12.25 |
| Laser pulse width | 10 fs |
| Absorption coefficient* | $6.7\times10^4$ cm$^{-1}$ |
| Reflectivity | 0.25 |

 ©2006 The American Physical Society

## II. EXPERIMENT AND SAMPLE

InAs wafers with different doping concentrations are used as THz sources in a THz time-domain spectroscopy system at room temperature. The doping concentrations of both the $n$- and $p$-type InAs samples vary from $1\times10^{16}$ to $2\times10^{18}$ cm$^{-3}$. All the wafer surfaces are well polished to minimize laser scattering. The Ti:sapphire laser (FemtoLasers, Inc.) used in the experiment has an average output power of 350 mW, pulse duration of 10 fs, pulse spectral width of 100 nm, repetition rate of 75 MHz, and central wavelength of 790 nm. The laser beam is directed onto the sample with an incident angle of 45° to the surface normal, and is focused on the surface with a beam diameter of 200 $\mu$m. The THz waves radiated from the InAs surface are collected and collimated within 14° collection angle by a pair of 4-in. parabolic mirrors and then focused on a 1 mm ZnTe crystal, directed through this detector crystal collinearly with the probe beam. Electro-optic (EO) sampling is used to register the THz signals.

## III. RESULTS AND DISCUSSION

Experimental evidence of THz radiation via the photo-Dember effect is based on the fact that THz electric fields radiated from $n$- and $p$-type InAs have the same polarity.[6] The same THz wave polarity contradicts the mechanism of surface-field-induced THz wave generation, since the surface band bending for many $n$-type and $p$-type semiconductors are opposite. For instance, the surface band bending in an $n$-type GaAs is upward while it is downward in a $p$-type GaAs. The directions of photocarriers transport in these GaAs surfaces are therefore opposite and the generated THz waves will show opposite polarity. However, due to the formation of an accumulation layer on the surface of an InAs wafer, which pins the surface Fermi level above conduction band minimum, the surface band bending for both $n$- and $p$-type InAs are downward, same as a $p$-type GaAs. An argument is raised that the same THz wave polarity from $n$- and $p$-type InAs wafers is not sufficient to eliminate the possibility that the THz radiation from InAs wafer is triggered by the surface electric field. Furthermore, the THz wave polarities from both $n$- and $p$-type InAs should be the same as a $p$-type GaAs if the THz radiations from InAs are attributed to surface band bending. To check this assumption, the polarity of THz waves from InAs wafers is compared with $n$- and $p$-type GaAs wafers in Fig. 1. Both the $n$- and $p$-type InAs show THz wave polarity the same as the $n$-type GaAs. It suggests that the mechanism of THz radiation from InAs wafer is mainly due to the photo-Dember effect.

There are several methods for calculating the carrier drift-diffusion and THz radiation such as drift-diffusion equation, Monte Carlo method,[7,13] and quantum mechanics.[14] Those methods have been applied in solving the THz generation from GaAs and InP due to the surface field excitation. We use the drift-diffusion equation (DDE) to investigate the process of THz wave radiation from InAs surfaces contributed by photo-Dember effect, and discuss the dependence of THz wave generation with doping concentration. DDE is one of the simplest formulations of the Boltzmann transport equation that give a quantitative analysis of photoexcited carrier dynamics. It has been used to simulate the carrier dynamics in the surface electric field of GaAs (Ref. 15) and THz wave generation in $n$-type GaAs (Refs. 3 and 4) and InP.[5] By solving simultaneously the continuity equation of the carriers and the Poisson equation, we are able to find quantitatively the carrier concentration distribution and temporal evolution, together with the transient current and electric field evolution

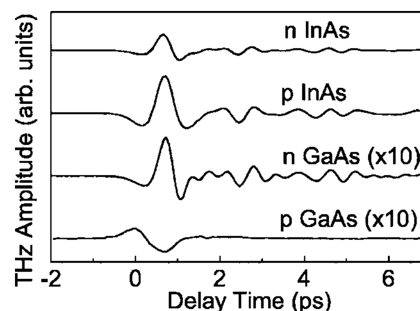


FIG. 1. THz waveform generated from $n$-type InAs (doping concentration is $3\times10^{16}$ cm$^{-3}$), $p$-type InAs (doping concentration is $1\times10^{16}$ cm$^{-3}$), $n$-type GaAs (doping concentration is $3\times10^{17}$ cm$^{-3}$), $p$-type GaAs (doping concentration is $3\times10^{17}$ cm$^{-3}$), respectively.

$$\frac{\partial N_i(z,t)}{\partial t} = G(z,t) + \frac{\partial}{\partial z}\left\{ D_i(z,t)\frac{\partial N_i(z,t)}{\partial z}\right\} \pm \frac{\partial}{\partial z}\{\mu_i(z,t)E(z,t)N_i(z,t)\}, \tag{1}$$

$$\frac{\partial E(z,t)}{\partial z} = \frac{e}{\varepsilon_0\varepsilon_S}\{N_h(z,t) - N_e(z,t) \pm N_a(z,t)\}. \tag{2}$$

Here $N_i(z,t)$ is the carrier concentration ($i=e,h$ indicate electrons and holes, respectively), $N_a(z,t)$ is the doping concentration, $G(z,t)=I(t)\alpha(1-R)e^{-\alpha z}$ is the photoexcitation term, $I(t)$ is the laser intensity with the Gaussian temporal waveform, and a full width half maximum (FWHM) of 10 fs. $\alpha$ is the inverse of the penetration depth in InAs which is 150 nm for the 800 nm laser beam. The surface reflection $R$ for the 800 nm laser beam on InAs surface is about 25%. Based on experimental conditions, we set the photo excitation density on the surface at $10^{14}$ cm$^{-2}$ and assume the efficiency of photoexcitation is 1. $E(z,t)$ is the electric field distribution induced by the spatial separation of the electrons and holes. $D_i$ and $\mu_i$ are diffusion constant and the mobility of the carriers, respectively. Their relationships are given by the diffusion constant and the Einstein relation $D_i=k_BT_c\mu_i/e$. More parameters for the simulation are listed in Table I.

From Eq. (1) it is seen that the carriers on the semiconductor surface tend to drift and diffuse simultaneously and either of these movements contribute to the THz radiation. GaAs has been reported to radiate THz waves dominated by drift currents for a low carriers' excess energy ($h\upsilon$=1.5 eV) but dominated by diffusion currents for a high carriers' excess energy ($h\upsilon$=3.1 eV).[16] Since the bandgap of InAs is only 0.35 eV, which is much smaller than that of GaAs, the

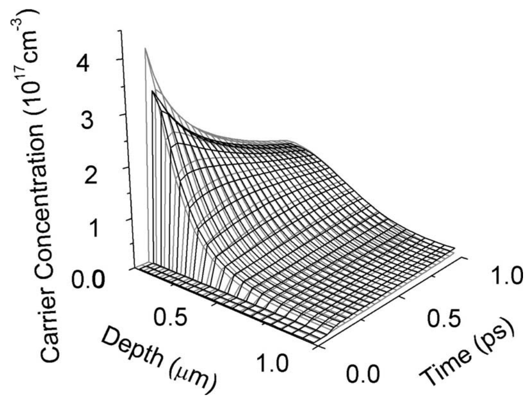


FIG. 2. A three-dimensional spatial and temporal carrier concentration distribution of photoexcited electrons and holes at the InAs surface. The gray curves represent electron distribution and the dark curves represent the hole distribution.

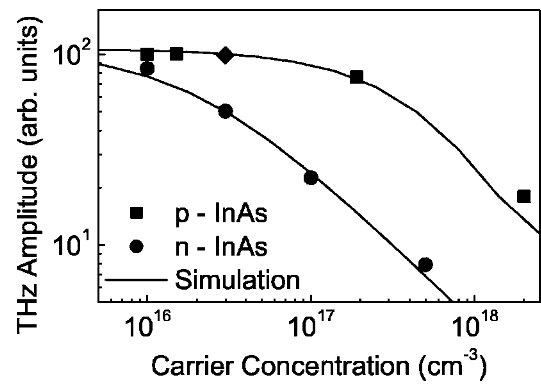


FIG. 3. Experimental and theoretical results of THz wave radiation versus increased doping concentration. The squares represent the THz wave amplitude from $p$-type (100) InAs, and the dots represent THz wave amplitude from $n$-type (100) InAs. The diamond represents the THz wave amplitude from a $p$-type (111) InAs with a carrier concentration at $3 \times 10^{16}$ cm$^{-3}$. The curves are the calculated results.

carriers' excess energy of InAs is expected much larger than GaAs when the energy of incident photons is 1.5 eV. The THz radiations from InAs using Ti:sapphire laser should therefore be dominated by diffusion current.

There are two processes of photocarrier dynamics after a femtosecond beam injects onto the InAs surface: carrier thermalization and carrier cooling. The hole thermalization and cooling in InAs is much faster than that of electrons due to the frequent scattering and interaction between the hole and other carriers and phonons.[17] Also, the mobility of the holes are several tenth times smaller compared to that of the electrons in InAs, therefore the effect of the holes diffusion and drift could be much slower than that of the electrons. The quick change of temperature on the holes will not significantly change their drift and diffusion action compared with the fast transport of the electrons. In order to simplify our calculation we assume that the temperature of the photogenerated holes is invariant during these processes. It is known that the thermalization of photogenerated electrons in InAs occurs with a characteristic time on the order of hundreds femtoseconds. If we take this factor into consideration, the calculated THz waveform will consequently be longer than the waveform without considering this factor. However, this factor will not qualitatively change our result on comparing THz wave amplitude with different doping concentration. According to Hansei *et al.*,[17] the cooling of the electron will last over several picosecond time scales. This process is long enough compared to the processes of THz wave radiation and time window for our calculation. To simplify our model for drift diffusion equation, we consider electrons and holes are in quasi-equilibrium, the photoexcited electrons temperatures are constantly at 6000 K (0.5 eV), photoexcited holes constantly at room temperature.

Figure 2 shows the spatiotemporal distribution of photogenerated electrons and holes within 1 ps evolution and within the depth of 1 $\mu$m under the surface of InAs. The gray grid represents the photoexcited electron distribution and the dark grid represents the photoexcited hole distribution. After the laser beam is injected, the number of photogenerated electrons and holes increases drastically, with an exponential decrease spatially. Then, due to the large gradient of the carrier distribution, these carriers diffuse toward the interior of the InAs. The carrier concentration nearest to the surface will drop down. The concentration of electrons near the surface drops down faster than that of holes, since the mobility of the electrons is much higher than that of the holes. The subsequent spatial difference of the electron and hole distribution generates a photo-Dember electric field. The existence of the field causes the drift action of the electron and holes toward each other, which will reduce the spatial difference. The sudden rising of the photogenerated electrons and their movement afterwards could trigger the THz wave radiation. The electric field of the THz wave is given by $E_{\mathrm{THz}} \propto \partial J / \partial t$, while $J$ is the current induced from the photogenerated electrons and holes.

Figure 3 shows the comparison of THz wave signal generated from a series of $n$- and $p$-type InAs wafers, with the doping concentrations of the InAs wafers varying from $1 \times 10^{16}$ cm$^{-3}$ to $2 \times 10^{18}$ cm$^{-3}$. The squares represent the THz wave peak amplitude from $p$-type InAs wafers, while the dots represent the THz wave peak amplitude from $n$-type InAs wafers. The curves represent the corresponding DDE simulation and it matches well with the experimental data. It is seen from this figure that a $p$-type InAs has a higher THz radiation efficiency compared with an $n$-type InAs wafer at the same carrier concentration. The THz radiations from both $n$- and $p$-type InAs wafers increase with decreasing carrier concentration. At very low carrier concentration around $10^{16}$ cm$^{-3}$, the THz wave signal from $n$-type InAs is nearly 70 to 80% that from $p$-type InAs. Also it is worthy to note that the THz wave signal from $p$-type InAs only decreases slightly by increasing the carrier concentration from $1 \times 10^{16}$ to $3 \times 10^{16}$ cm$^{-3}$, and then decreases significantly as carrier concentration increases. As a comparison, the THz wave generated from $n$-type InAs at a low doping concentration decreases more prominently by increasing the doping concentration. Therefore, at higher doping concentrations, the THz wave signals from $n$- and $p$-type InAs with the same carrier concentration will show amplitude difference for several times. The amplitude of the signals from the $p$-type InAs

with a doping concentration of $1\times10^{16}$ cm$^{-3}$ and the $n$-type InAs with a doping concentration of $2\times10^{18}$ cm$^{-3}$ could even differ by a factor of more than 10. One piece of $p$-type InAs with doping concentration $3\times10^{16}$ cm$^{-3}$ in the experiment is (111) oriented. As shown in Fig. 3, the THz amplitude for the portion induced by photo-Dember effect of this sample is represented by a diamond. A discussion of it will be detailed later.

In order to understand why the THz signal decreases with increasing doping concentration of both $n$- and $p$-type InAs, we rewrite Eq. (1) as

$$\frac{\partial \Delta N_i(z,t)}{\partial t} = G(z,t) + \frac{\partial}{\partial z}\left\{ D_i(z,t)\frac{\partial \Delta N_i(z,t)}{\partial z}\right\} \pm \frac{\partial}{\partial z}\{\mu_{i,c}(z,t)E(z,t)N_{i,0}(z,t) + \mu_{i,h}(z,t)E(z,t)\Delta N_i(z,t)\}. \quad (3)$$

In this equation $N(z,t)$ is replaced by $N(z,t) = N_{i,0}(z,t)+\Delta N_i(z,t)$, $N_{i,0}(z,t)$ represents the cold or doping electron and holes concentration, while $\Delta N_i(z,t)$ represents the hot or photoexcited carrier concentration. Also $\mu_{i,c}(z,t)$ represents the mobility for cold carriers and $\mu_{i,h}(z,t)$ represents the mobility for hot carriers. The first part on right side of the equation represents the injection of photocarriers. The injected photon excitation density is incorporated into this part to reflect the photoexcitation. The second part on the right side represents the diffusion action of the photoexcited carriers. The third part can also be separated into two parts. One part is the drift action of the photocarriers and the other is the drift action of the doped carriers in an electric field. From this equation we can see that both doped and photoexcited electrons and holes participate in the carrier redistribution in the drift action. However, although all the carriers statistically join the diffusion action, only the amount of carriers that form the gradient of the carrier concentration will have an actual effect on the diffusion action. The higher the carrier concentration of the InAs wafers, the more doped carriers that will join in the redistribution of the carrier concentration via drift action. Therefore, for $n$-type InAs with a higher carrier concentration, more doped electrons join the drift action in the opposite direction of electron diffusion. Their participation will greatly weaken or "screen" the photo-Dember field and consequently weaken the THz wave radiation. For the same reason, we see that $p$-type InAs with a lower doping concentration generates higher amplitude THz waves than the InAs with a higher carrier concentration. In comparing $n$- and $p$-type InAs with the same doping concentration, the screening of the $n$-type InAs is mainly from the large amount of doped electrons, which have a much higher mobility than holes, while $p$-type InAs has its screening from the large amount of doped holes. Therefore, the effect of screening by electrons in $n$-type InAs is stronger than the effect caused by the holes in $p$-type InAs.

The transport of the charges can be clearly presented by examining the spatial difference of the carrier concentration between the electrons and holes. We refer to this difference $n(x)-p(x)$ as net charge distribution. Figure 4 shows the net charge distribution of InAs wafers with a doping concentration at $1\times10^{16}$ cm$^{-3}$ ($p$-type, solid curve) and $1\times10^{18}$ cm$^{-3}$ ($n$-type, dash curve). Time zero refers to the time when the laser pulse reaches its maximum. At time −50 fs, before the laser pulse arrives, the net charge distribution is zero within the surface. The electrons and holes are in statistical equilibrium. At 50 fs after the laser pulse arrives, the net charge distribution of a low doping InAs surface within 250 nm is much smaller than that of a higher doping InAs and after 250 nm is much larger than that of a higher doping InAs. This means that the spatial separation of the electrons and holes in low doping InAs is larger than in the higher doping InAs. As time evolves, it is seen that the positive part of the net charge distribution diffuses towards the interior of the sample, and the diffusion speed of the low doping InAs appears to be faster than that of the high doping InAs. That is a direct proof of how doped carriers influence the drift movements statistically.

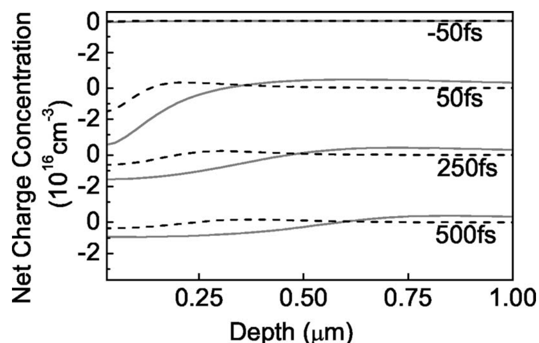


FIG. 4. Calculation of net charge distribution at the InAs surface at −50, 50, 250, 500 fs, top to bottom, respectively. The solid lines represent the $p$-type InAs with a doping concentration at $1\times10^{16}$ cm$^{-3}$, and the dotted lines represent the $n$-type InAs with a doping concentration at $1\times10^{18}$ cm$^{-3}$.

Figure 5 shows the photogenerated electric field from electron-hole separation. The solid and dotted curves represent a $p$-type $1\times10^{16}$ cm$^{-3}$ InAs and an $n$-type $1\times10^{18}$ cm$^{-3}$ InAs. It shows that the $p$-type InAs with low

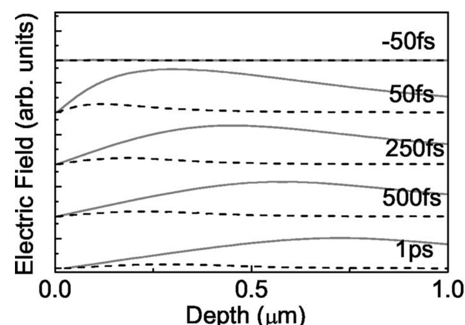


FIG. 5. Calculation of the photo-Dember electric field at the InAs surface as time evolved at −50, 50, 250, 500 fs, and 1 ps top to bottom, respectively. The electric field is generated by the spatial difference between the photoexcited electrons and the holes. The solid lines represent the $p$-type InAs with doping concentration at $1\times10^{16}$ cm$^{-3}$, and the dotted lines represent the $n$-type InAs with doping concentration at $1\times10^{18}$ cm$^{-3}$.

carrier concentration generates a larger electric field than InAs with a higher concentration. The peak of the electric field decreases as time evolves and shifts toward the interior of the semiconductor surface. This is also consistent with the different diffusion speed of carriers with different carrier concentrations.

There are several points worth noting in these results. First is the temperature of the electrons and holes. The mobility of the doping electrons and holes are dependent on many factors such as the lattice temperature, the carrier temperature, exterior electric field and doping concentration, etc.[18–21] Unfortunately, it is difficult to experimentally determine the mobility of the photoexcited electrons and holes. Upon the injection of the laser beam onto the InAs, the temperature of the photoexcited carriers depends on the excess energy of the photoexcitation. In our experiments, the transient photoexcited temperature will reach 6000 K, while the lattice temperature increases relatively little compared with the drastic change of the electron temperature. Therefore, the diffusion constant of the photoexcited electrons will change greatly due to the high electron temperature. It seemed that our conclusion regarding THz wave signals versus the doping concentrations would not change qualitatively by considering the mobility dependence either on the doping concentration or the lattice temperature, because these changes in the mobility are relatively smaller compared with the orders of magnitude increase of the doping concentration. Second, it is reported that the effective mass of electrons will increase gradually with an increase in the carrier concentration. Thus the mobility will decrease with increasing carrier concentration.[18] However, this effect is prominent mainly at low temperature. At room temperature the change of the mobility is not a dominant factor. Third, A $p$-type InAs is reported to have an accumulation layer[22,23] at the surface. The thickness of this accumulation layer is about 10 nm. In our simulation we did not consider this factor, since it is very thin compared with the penetration depth of the laser pulse in InAs. Fourth, the excitation of InAs with 1.5 eV photons may cause the electron being scattered into the $L$ valley, whose energy is 1.08 eV above the valence band. However, the rest energy of excitation will be shared by electron and hole. It has been reported that the rest energy of the photoexcited electron is 0.5 eV. It is relatively small compared with the barrier between the $L$ and $\Gamma$ valley and statistically the intervalley scattering will not be significant. As a result we did not consider the interband scattering in our model since it will not qualitatively change our conclusion of the dependence of THz wave amplitude on the carrier concentration of InAs. When the interband scattering is considered, the $L$-valley scattering will enhance the electron mass and therefore decrease the electron mobility, which will make the actual THz radiation value slightly less than what we predicted here. However, it also will not qualitatively change our conclusion on the dependence of THz wave amplitude on the carrier concentration of InAs.

Now we check (111) InAs and its THz wave radiation. Figure 6 shows the azimuthal dependence of THz wave radiation from a (100) and (111) $p$-type InAs at a 45° incident angle. The dots show the experimental data and the lines fit the experimental data with a cosine function. The doping concentration of (100) InAs is $1\times10^{16}$ cm$^{-3}$ while the (111) InAs is $3\times10^{16}$ cm$^{-3}$. From calculated results in Fig. 3 that THz waves from the photo-Dember effect are close in amplitude for $p$-type InAs with doping concentration between $1\times10^{16}$ cm$^{-3}$ and $3\times10^{16}$ cm$^{-3}$.

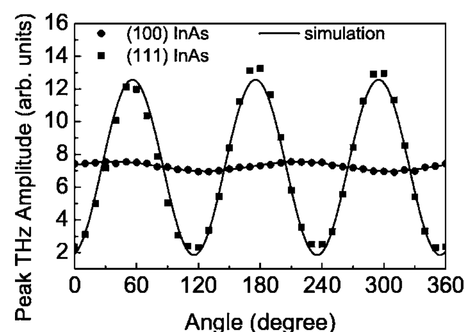


FIG. 6. The azimuthal dependence of THz wave generation from multi-oriented InAs surfaces. The squares represent the experimental measurements of THz wave amplitude from a (111) oriented $p$-type InAs with a doping concentration at $3\times10^{16}$ cm$^{-3}$, while the dots represent the experimental data of THz wave amplitude from a (100) oriented $p$-type InAs with a doping concentration at $1\times10^{16}$ cm$^{-3}$. The curves represent the fitting results by cosine equations.

In Fig 6, both samples show azimuthally angle-dependent THz wave amplitude, which could be evaluated with $E_{\mathrm{peak}}=E_{\mathrm{Dember}}+E_{\mathrm{opt\ rectification}}\cdot\cos(\omega\theta)$. It is clear to see that both the samples have an $E_{\mathrm{Dember}}$ component with nearly the same value. These components are contributed by the photo-Dember effect. Also in Fig. 3, the diamond presents the $E_{\mathrm{Dember}}$ component of THz radiation from the (111) oriented sample. The differently oriented InAs have about the same $E_{\mathrm{Dember}}$ component, which is consistent with our conclusion based on the photo-Dember effect. The $E_{\mathrm{opt\ rectification}}\cos(\omega\theta)$ component, contributed by the optical rectification, is quite different between these two samples. The azimuthal dependence of the THz radiation in (111) oriented InAs is obvious with a period of $\pi/3$; while a tilted (100) oriented InAs has a slight azimuthal dependence in THz radiation with a period of $\pi/2$. These experiments comply with previous studies of THz radiation processes via optical rectification from other zinc-blende crystals. In our experiment the THz wave amplitude from optical rectification components and photo-Dember components are in the same order. The strong THz radiation by a nonlinear effect could possibly be due to the field enhanced $\chi^{(2)}$ process, which has been studied.[11]

Furthermore the THz wave emission from InAs wafer will be enhanced magnitudes stronger[24] by applying an intense magnetic field perpendicular to the surface normal of the InAs wafer. The magnetic field could change the orientation of the carrier transports and therefore change the output orientation of the THz radiation; however, it has no effect on optical rectification since there is no carrier transport participating in the THz radiation. Our observation with a (111) oriented InAs emitter in the magnetic field corresponds well with this statement.

## IV. CONCLUSION

In conclusion, we reported that the experimental and theoretical results of our systematic study of THz wave radia-

tion from InAs wafers with femtosecond optical pulses indicate that the low carrier concentration wafers are more suitable for THz wave generation. This relationship of THz radiation versus the carrier concentration agrees well with the theory of the screened photo-Dember effect. With a comparable carrier concentration and identical optical excitation, a *p*-type InAs works more effectively than an *n*-type InAs. A *p*-type InAs ($1\times10^{16}$ cm$^{-3}$) is the strongest unbiased semiconductor emitter we have ever tested with a Ti:sapphire laser oscillator. We discussed the screening characteristics of cold electrons as they participate in the drift movement upon a transient electric field driven by the laser pulses.

## ACKNOWLEDGMENTS

This work was partially supported by the National Science Foundation and the Army Research Office. Kai Liu thanks IMRA America Inc. for the IMRA Fellowship and OIDA Photonics Technology Access Program Award. We thank Ishawara Bhat for providing Hall measurements. We thank Krishna Mandal for providing sample wafers and Arunas Krotkus for sample provisions and valuable discussions.

*Email address: zhangxc@rpi.edu

[1] X.-C. Zhang and D. H. Auston, J. Appl. Phys. **71**, 326 (1992).
[2] T. Dekorsy, H. Auer, H. J. Bakker, H. G. Roskos, and H. Kurz, Phys. Rev. B **53**, 4005 (1996).
[3] R. Kersting, J. N. Heyman, G. Strasser, and K. Unterrainer, Phys. Rev. B **58**, 4553 (1998).
[4] R. Kersting, K. Unterrainer, G. Strasser, H. F. Kauffmann, and E. Gornik, Phys. Rev. Lett. **79**, 3038 (1997).
[5] M. Nakajima, M. Hangyo, M. Ohta, and H. Miyazaki, Phys. Rev. B **67**, 195308 (2003).
[6] P. Gu, M. Tani, S. Kono, K. Sakai, and X.-C. Zhang, J. Appl. Phys. **91**, 5533 (2002).
[7] M. B. Johnston, D. M. Whittaker, A. Corchia, A. G. Davies, and E. H. Linfield, Phys. Rev. B **65**, 165301 (2002).
[8] N. Sarukura, H. Ohtake, S. Izumida, and Z. Liu, J. Appl. Phys. **84**, 654 (1998).
[9] H. Takahashi, A. Quema, M. Goto, S. Ono, and N. Sarukura, Jpn. J. Appl. Phys., Part 2 **42**, L1259 (2003).
[10] H. Ohtake, H. Murakami, T. Yano, Shingo Ono, N. Sarukura, H. Takahashi, Y. Suzuki, G. Nishijima, and K. Watanabe, Appl. Phys. Lett. **82**, 1164 (2003).
[11] R. Adomavicius, A. Urbanowicz, G. Molis, A. Krotkus, and E. Satkovskis, Appl. Phys. Lett. **85**, 2463 (2004).
[12] S. L. Chuang, S. Schmitt-Rink, B. I. Greene, P. N. Saeta, and A. F. J. Levi, Phys. Rev. Lett. **68**, 102 (1992).
[13] G. Satyanadh, R. P. Joshi, N. Abedin, and U. Singh, J. Appl. Phys. **91**, 1331 (2002).
[14] G. Meinert, L. Banyai, P. Gartner, and H. Haug, Phys. Rev. B **62**, 5003 (2000).
[15] T. Dekorsy, T. Pfeifer, W. Kutt, and H. Kurz, Phys. Rev. B **47**, 3842 (1993).
[16] J. N. Heyman, N. Coates, and A. Reinhardt, Appl. Phys. Lett. **83**, 5476 (2003).
[17] H. Nansei, S. Tomimoto, S. Saito, and T. Suemoto, Phys. Rev. B **59**, 8015 (1999).
[18] V. W. L. Chin, R. J. Egan, and T. L. Tansley, J. Appl. Phys. **72**, 1410 (1992).
[19] R. C. Curby and D. K. Ferry, Phys. Rev. B **3**, 3379 (1971).
[20] D. L. Rode, Phys. Rev. B **3**, 3287 (1971).
[21] D. L. Rode, Phys. Rev. B **2**, 1012 (1970).
[22] T. D. Veal and C. F. McConville, Phys. Rev. B **64**, 085311 (2001).
[23] Shuma Abe, Takeshi Inaoka, and Masayuki Hasegawa, Phys. Rev. B **66**, 205309 (2002).
[24] N. Sarukura, H. Ohtake, S. Izumida, and Z. Liu, J. Appl. Phys. **84**, 654 (1998).